IEEE Photonics Journal
An IEEE Photonics Society Publication

High Nonlinearity and Single-Mode Transmission in Tapered Multimode As_2Se_3-PMMA Fibers

Volume 4, Number 3, July 2012

Chams Baker
Martin Rochette

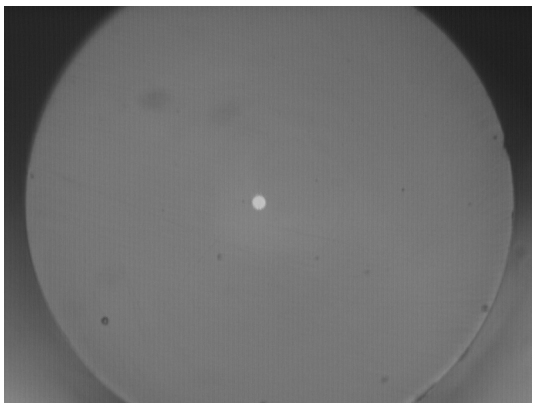

DOI: 10.1109/JPHOT.2012.2202103
1943-0655/$31.00 ©2012 IEEE

IEEE photonics SOCIETY

IEEE

High Nonlinearity and Single-Mode Transmission in Tapered Multimode As_2Se_3-PMMA Fibers

Chams Baker and Martin Rochette

McGill University, Department of Electrical and Computer Engineering, Montréal, QC H3A 2A7, Canada

DOI: 10.1109/JPHOT.2012.2202103
1943-0655/$31.00 ©2012 IEEE

Manuscript received April 25, 2012; revised May 21, 2012; accepted May 22, 2012. Date of current version June 5, 2012. This work was supported by the Natural Sciences and Engineering Research council of Canada and the Fonds de Recherche Nature et Technologies du Québec. Corresponding author: C. Baker (e-mail: chams.baker@mail.mcgill.ca).

Abstract: We demonstrate the fabrication and use of a 10-cm-long As_2Se_3-PMMA microwire with ultrahigh waveguide nonlinearity $\gamma = 176\ W^{-1}m^{-1}$ that is fully compatible with standard single-mode silica fibers. The fabrication of this microtaper is simplified with respect to a previous approach as the core is made of a bulk As_2Se_3 cylinder rather than a single-mode step-index As_2Se_3 fiber. The successful operation of this nonlinear component is demonstrated with a Kerr-shutter switching experiment based on nonlinear polarization rotation.

Index Terms: Nonlinear, Kerr effect, fabrication and characterization, photonic materials.

1. Introduction

Devices based on the nonlinear Kerr effect enable a wide range of all-optical processing applications such as switching [1], wavelength conversion [2], supercontinuum generation [3], and signal regeneration [4]. For pulses that propagate in a waveguide, the Kerr effect generates a time-dependent nonlinear phase-shift $\phi(t)$ with a maximum phase-shift $\phi_{SPM} = \gamma P_0 L_{eff}$, where $\gamma = k_0 n_2 / A_{eff}$ is the waveguide nonlinearity, P_0 is the peak power of the pulse, $L_{eff} = (1 - e^{-\alpha L})/\alpha$ is the effective length of the nonlinear waveguide, L is the length of the waveguide, α is the loss coefficient, A_{eff} is the modal effective area, n_2 is the material nonlinearity, $k_0 = 2\pi/\lambda$ is the wavenumber, and λ is the wavelength [5]. For a practical implementation of devices based on nonlinear effects, it is desirable to use a nonlinear medium with γ as high as possible such that a given ϕ_{SPM} can be achieved with a low power consumption (low P_0) and in a compact device (short L_{eff}).

In one approach for increasing γ, materials with high n_2 such as chalcogenide glasses [6] and doped glasses [7] have been used. In another approach, microwires with a large core to cladding refractive index contrast [8], photonic crystal fibers [3], [9], and suspended-core optical fibers [10] have been used to reduce A_{eff}. Microwires [11], [12], photonic crystal fibers [13], and suspended-core fibers [14] made of chalcogenide glass combine both aforementioned approaches and thus achieve among the largest values of γ available in glasses.

The first designs toward the fabrication of chalcogenide microwires were air-surrounded microwires [11]. Similar to photonic crystal and suspended-core fibers made of chalcogenide glasses [13], [14], such microwires are highly nonlinear and have an engineerable chromatic dispersion. However, chalcogenide microwires are prone to rupture due to their thin structure and

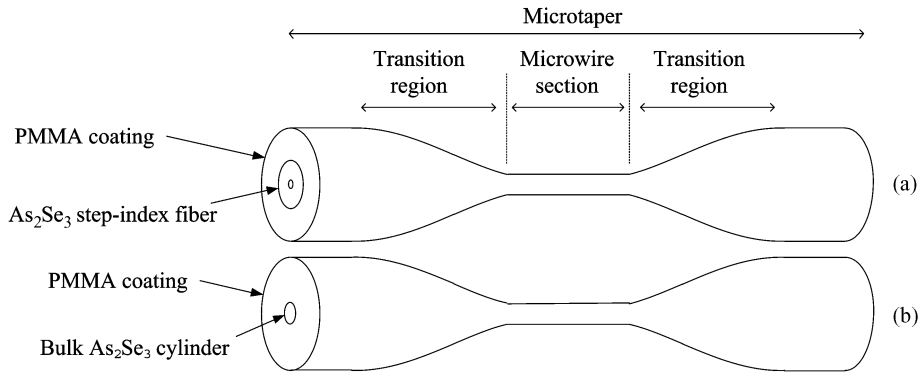

Fig. 1. Schematic of hybrid microtapers. (a) Hybrid microtaper with a PMMA coated single-mode step-index As_2Se_3 fiber. (b) Hybrid microtaper with a PMMA coated bulk As_2Se_3 cylinder.

must be used in a dust free or controlled environment because ~9% of the fundamental mode propagates outside the microwire.

Chalcogenide glasses have been combined with polymers, tellurite, and silica to form photonic fiber structures for a variety of applications. A Bragg fiber composed of alternating chalcogenide-polymer layers surrounding a polymer core have been fabricated to guide CO_2 laser light [15]–[17]. A photonic crystal fiber composed of a chalcogenide core and a holey tellurite cladding has been fabricated and used for supercontinuum generation [18]. More recently, a fiber with a chalcogenide core and a silica cladding has been used for supercontinuum generation in the near infrared [19].

In 2010, we have reported the fabrication and optical characterization of the first hybrid As_2Se_3-PMMA microtaper, prepared by tapering a single-mode step-index As_2Se_3 fiber that is coated with a PMMA layer [12]. Fig. 1(a) presents a schematic of the hybrid microtaper fabricated from a PMMA coated step-index As_2Se_3 fiber. With this material combination, the As_2Se_3 core of the microwire provides a large nonlinearity whereas the PMMA coating ensures mechanical robustness and flexibility to the assembly for normal handling as well as limiting the evanescent interaction with the environment. In the fabrication process of the hybrid microwire, a single-mode step-index As_2Se_3 fiber is used to ensure single-mode propagation from the fiber input to the microwire and from the microwire back to the fiber output, given that the taper transition region satisfies the adiabaticity criteria [20], [21]. In this case though, the transmission of the resulting hybrid microwire depends upon the As_2Se_3 fiber quality and design.

Hybrid microtapers with single-mode transmission can also be fabricated from a multimode As_2Se_3-PMMA fiber composed of a bulk As_2Se_3 cylinder that is coated with a PMMA layer, as presented in Fig. 1(b). The multimode hybrid fiber must be tapered sufficiently such that only the fundamental mode is preserved in the As_2Se_3 core of the microwire. Single-mode transmission in tapered multimode fiber structures was first observed and studied in tapered fused couplers [22], [23]. Later, different tapering schemes have been used to filter out higher order modes in multimode fibers and achieve single-mode transmission [24]–[26].

In this paper, we report single-mode transmission and high nonlinearity in tapered multimode As_2Se_3-PMMA fibers. We fabricate multimode and large refractive index contrast hybrid fibers with an As_2Se_3 core and a PMMA cladding. The As_2Se_3 core diameter is designed for optimal coupling between the fundamental mode of the hybrid fiber and the fundamental mode of a standard single-mode silica fiber (SMF). A segment of this multimode fiber is then tapered down into a wire until the As_2Se_3 core sustains single-mode transmission. This microwire with SMF-compatible pigtails is then characterized and used as the nonlinear element of a Kerr-shutter to achieve optical switching based on nonlinear polarization rotation [27].

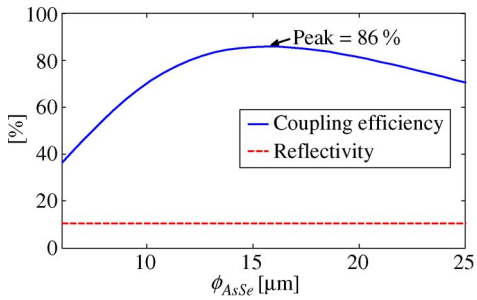

Fig. 2. Calculated coupling efficiency and reflectivity as a function of the As_2Se_3 core diameter.

2. Multimode AsSe-PMMA Fiber Design

A primary design criterion for the As_2Se_3-PMMA multimode fiber is the maximization of the coupling efficiency between the fundamental mode of an SMF and the fundamental mode of the hybrid fiber. The coupling efficiency and the reflectivity are calculated using [28]

$$\eta = \frac{4\beta_i\beta_t}{(\beta_i+\beta_t)^2}\frac{\left[\int\int \vec{E}_t\vec{E}_i^* dxdy\right]^2}{\left[\int\int \vec{E}_t\vec{E}_t^* dxdy\right]\left[\int\int \vec{E}_i\vec{E}_i^* dxdy\right]}$$

$$R = \frac{(\beta_i-\beta_t)^2}{(\beta_i+\beta_t)^2}$$

where β, $\vec{E}$ are the propagation constant and the electric field distribution of the fundamental mode, and the subscripts i and t stand for the incident and transmitted light. Fig. 2 shows the coupling efficiency and the reflectivity as a function of the As_2Se_3 core diameter (ϕ_{AsSe}). Optimal coupling is achieved when $\phi_{AsSe} = 15.5$ μm with a coupling loss of 0.66 dB per facet from which 0.46 dB is due to reflection and the remaining 0.2 dB is due to mode mismatch. In practice, there are other sources of loss such as lateral misalignment between the cores, a gap between the facets of the two fibers, angular misalignment between the axes of the two fibers, a scratched fiber facet, a non planar fiber facet, or an angled facet, which lead to extra loss at each coupling facet.

3. Microtaper Design

To achieve single-mode transmission in tapered multimode As_2Se_3-PMMA fibers, the wire section must exclusively confine the fundamental mode. Moreover, there must be no power transfer between the fundamental mode and higher order modes in the transition region and multimode section of the taper. The wire section exclusively confine the fundamental mode when $\phi_{AsSe} \leq 0.49$ μm which corresponds to a normalized frequency $V = \pi\phi_{AsSe}(n_{AsSe}^2 - n_{PMMA}^2)^{0.5}/\lambda \leq 2.4$ [29], where n_{AsSe} and n_{PMMA} are the refractive indices of the As_2Se_3 core and the PMMA cladding, respectively. Moreover, to avoid power transfer between the fundamental mode and higher order modes there must be no sharp bends in the multimode section of the taper, and the slope of the taper transition region must satisfy the condition

$$\frac{d\phi_{AsSe}}{dz} < \frac{\phi_{AsSe}}{2\pi}(\beta_{11} - \beta_{12})$$

where β_{11} and β_{12} are the propagation constants of the modes HE_{11} and HE_{12}, respectively. Fig. 3 shows the maximum allowed taper slope for every value of the core diameter, also known as the delineation line. If the taper slope is made equal to the delineation line, the transition region over which ϕ_{AsSe} decreases from 15.5 μm to 0.49 μm can be made shorter than 1.0 mm. For practical reasons and to guarantee an adiabatic propagation of the fundamental mode in the transition

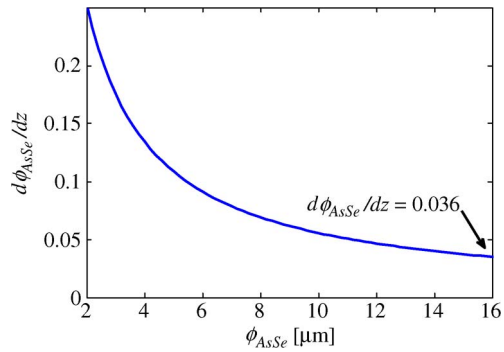

Fig. 3. Maximum allowed taper slope as a function of the As_2Se_3 core diameter for adiabatic transformation of the fundamental mode in the taper transition region.

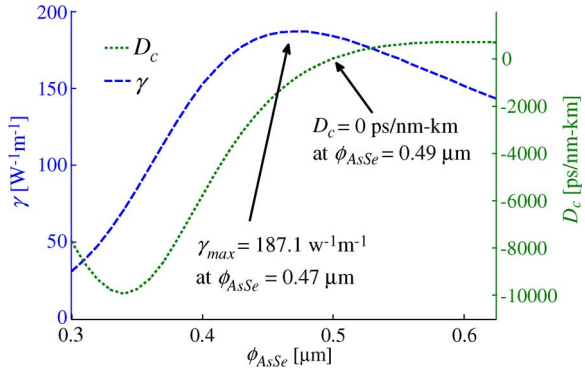

Fig. 4. Calculated waveguide nonlinearity parameter and chromatic dispersion of the hybrid microtaper as a function of the As_2Se_3 core diameter at a wavelength of 1550 nm.

region, the slope of the transition region from the initial diameter to the final diameter in the fabricated tapers is always set to $|d\phi_{AsSe}/dz| = \phi_{AsSe}/L_0$ with $L_0 = 1$ cm.

Determination of the chromatic dispersion and the waveguide nonlinearity involves solving the characteristic equation of an infinite cladding cylindrical waveguide to obtain the propagation constant β, the electric field distribution $\vec{E}$, and the magnetic field distribution $\vec{H}$ for the fundamental mode HE_{11} [29]. Solving the characteristic equation takes into account the wavelength dependence of the refractive index of As_2Se_3 obtained from the Sellmier relation $n^2_{AsSe}(\lambda) = 1 + \sum_{i=1}^{i=3} A_i^2\lambda^2/(\lambda^2 - \lambda_i^2)$ where $A_1 = 2.234921$, $A_2 = 0.347441$, $A_3 = 1.308575$, $\lambda_1 = 0.24164$ μm, $\lambda_2 = 19$ μm, and $\lambda_3 = 0.48328$ μm [30], and the refractive index of PMMA obtained from the Cauchy relation $n^2_{PMMA} = B_1 + B_2\lambda^2 + B_3\lambda^{-2} + B_4\lambda^{-4} + B_5\lambda^{-6} + B_6\lambda^{-8}$ where $B_1 = 2.399964$, $B_2 = -8.308636 \times 10^{-2}$, $B_3 = -1.919569 \times 10^{-1}$, $B_4 = +8.720608 \times 10^{-2}$, $B_5 = -1.666411 \times 10^{-2}$, and $B_6 = +1.169519 \times 10^{-3}$ [31], with λ being the wavelength in μm. Fig. 4 presents the chromatic dispersion (D_c) as a function of ϕ_{AsSe} calculated using $D_c = -(\lambda/c)(d^2n_{eff}/d\lambda^2)$ [5] where $n_{eff} = \beta/k_0$ with k_0 being the wavenumber. Also presented in Fig. 4 is γ as a function of ϕ_{AsSe} at $\lambda = 1550$ nm calculated using $\gamma = k_0\bar{n}_2/A_{eff}$ with $\bar{n}_2$ being the effective material nonlinearity given by [32], [33]

$$\bar{n}_2 = \frac{\varepsilon_0}{\mu_0}\frac{\iint_\infty n_0^2(x,y)n_2(x,y)\left(2|\vec{E}|^4 + |\vec{E}^2|^2\right)dA}{3\iint_\infty \left|[\vec{E}\times\vec{H}^*]\cdot\hat{z}\right|^2 dA}$$

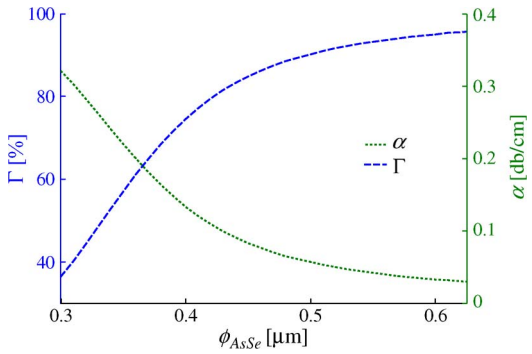

Fig. 5. Calculated confinement factor and loss of the hybrid microtaper as a function of the As_2Se_3 core diameter at a wavelength of 1550 nm.

and A_{eff} given by [32], [33]

$$A_{eff} = \frac{\left|\iint_{\infty}[\vec{E} \times \vec{H}^*] \cdot \hat{z}\, dA\right|^2}{\iint_{\infty}\left|[\vec{E} \times \vec{H}^*] \cdot \hat{z}\right|^2 dA}$$

where n_0 is the refractive index; n_2 is the material nonlinearity with $n_{2,AsSe} = 1.1 \times 10^{-17}$ m^2W^{-1} and $n_{2,PMMA} = -8 \times 10^{-19}$ m^2W^{-1} [6], [34]; ε_0 and μ_0 are the electric permittivity and the magnetic permeability of free space, respectively; z is the direction of propagation; and A is the transverse surface area. Fig. 4 shows that the optimal As_2Se_3 core diameter to achieve a maximum nonlinearity is $\phi_{AsSe} = 0.47$ μm for which $\gamma = 187.1$ $W^{-1}m^{-1}$.

Material losses in the hybrid microwire are calculated using $\alpha^{dB}_{hybrid} = \Gamma_{AsSe} \times \alpha^{dB}_{AsSe} + \Gamma_{PMMA} \times \alpha^{dB}_{PMMA}$, where $\Gamma_i = P_i/P_{tot}$ is the confinement factor with P_i being the power fraction of the mode in layer i and P_{tot} the total power of the mode. Fig. 5 presents the value of α^{dB}_{hybrid} as a function of ϕ_{AsSe} calculated using the attenuation coefficients $\alpha^{dB}_{AsSe} = 0.0085$ dB/cm [6] and $\alpha^{dB}_{PMMA} = 0.5$ dB/cm [35] at $\lambda = 1550$ nm. At the diameter of maximum nonlinearity $\phi_{AsSe} = 0.47$ μm the calculated α^{dB}_{hybrid} for the hybrid microwire is 0.069 dB/cm.

4. Hybrid Fiber and Microtaper Fabrication

Fig. 6(a) shows a schematic of the setup used for the fabrication of As_2Se_3-PMMA fiber preforms. A cylinder of bulk As_2Se_3 with a diameter of 170 μm is inserted into a commercially available PMMA tube with an inner diameter of 3.2 mm and an outer diameter of 9.5 mm and the assembly is pushed into a funnel heated at 230 °C at a constant feed velocity of $v_f = 50$ μm/s. The PMMA tube collapses on the As_2Se_3 cylinder and the composite flows out at the bottom of the funnel. The composite exiting from the bottom of the funnel is captured and is drawn at a constant velocity of $v_d = 225$ μm/s to obtain a preform with a uniform diameter. The preform is then drawn at a temperature of 200 °C to obtain a hybrid fiber with $\phi_{AsSe} = 15.5$ μm and $\phi_{PMMA} = 472.8$ μm.

A 6 cm long sample of this hybrid fiber is cut, and both ends are polished. Fig. 6(b) presents an image of the polished facet of the hybrid fiber showing the As_2Se_3 core surrounded by the PMMA cladding. The hybrid fiber sample is tapered using the heat-brush method [12], [23], [36], [37] to obtain a microwire with a $\phi_{AsSe} = 0.45$ μm, $\phi_{PMMA} = 13.7$ μm, and a length of $L_w = 10.0$ cm. With a PMMA layer sufficiently robust for manual handling, the microtaper is manually removed from the tapering setup and transferred to a butt-coupling setup. The input and the output of the microtaper are permanently butt-coupled to SMF-28 fibers using UV-cured epoxy. Finally, the pigtailed microtaper is manually packaged in box to obtain a ready-for-use nonlinear component.

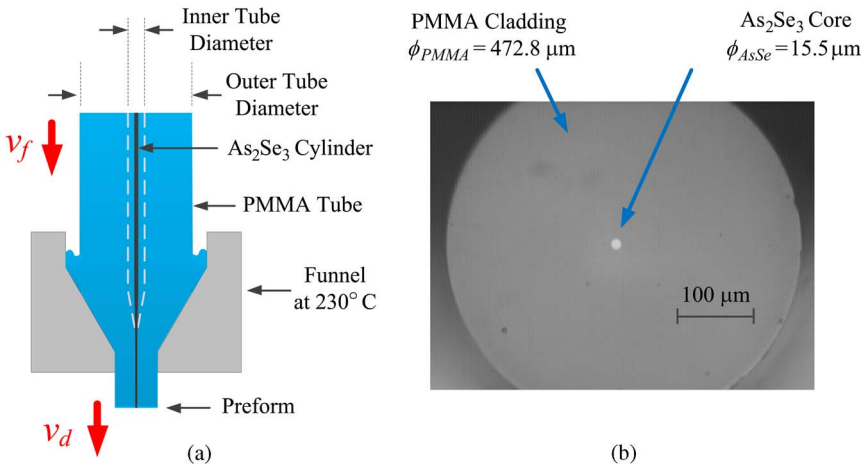

Fig. 6. (a) Schematic of the As_2Se_3-PMMA fiber preform fabrication setup and (b) an image of the hybrid fiber cross section.

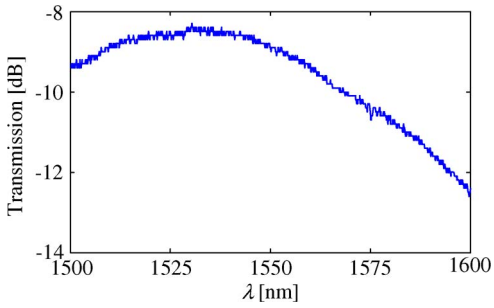

Fig. 7. Transmission spectrum of a hybrid microtaper with a wire length of 10 cm and a waist diameter of 0.45 μm.

5. Microtaper Characterization

Fig. 7 presents the transmission spectrum of the hybrid microtaper between $\lambda = 1500$ nm and $\lambda = 1600$ nm measured using amplified spontaneous emission noise from an Erbium-doped fiber amplifier and an optical spectrum analyzer with a resolution bandwidth of 0.06 nm. The transmission is maximum at $\lambda = 1530$ nm with a loss of 8.4 dB. The transmission decreases at shorter wavelengths because PMMA has an absorption peak at $\lambda = 1390$ nm and at longer wavelengths due to a combination of the presence of a PMMA absorption peak at $\lambda = 1620$ nm and the decrease of the mode confinement. The transmission spectrum of the microtaper has no interference features indicating single-mode transmission.

A loss coefficient of $\sim$0.52 dB/cm at $\lambda = 1530$ nm is experimentally estimated by the comparison between the transmission losses of multiple hybrid microtapers with identical transition regions and different wire section lengths. This measured loss is 6.3 times higher than the theoretically estimated loss of 0.083 dB/cm from Fig. 5. We believe the loss increase arises from imperfections in the fabrication process and the degradation of PMMA. Using the experimentally estimated value of the loss coefficient, propagation in the 10 cm long wire section of the microtaper amounts to 5.2 dB from the total 8.4 dB transmission loss at $\lambda = 1530$ nm in Fig. 7. The remaining 3.2 dB includes the losses from mode mismatch and reflection at the coupling interfaces (1.3 dB from Fig. 2), imperfections in the hybrid fiber facets, and propagation in the 3.5-cm-long transition regions of the microtaper.

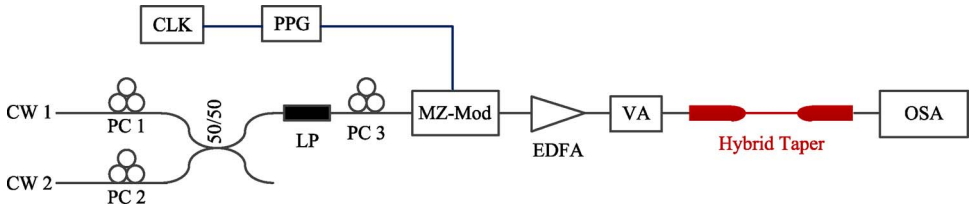

Fig. 8. Schematic of the waveguide nonlinearity measurement setup. CW: continuous wave laser, PC: polarization controller, LP: linear polarizer, CLK: electrical clock, PPG: pulse pattern generator, MZ-Mod: Mach–Zehnder modulator, EDFA: Erbium-doped fiber amplifier, VA: variable attenuator, OSA: Optical spectrum analyzer.

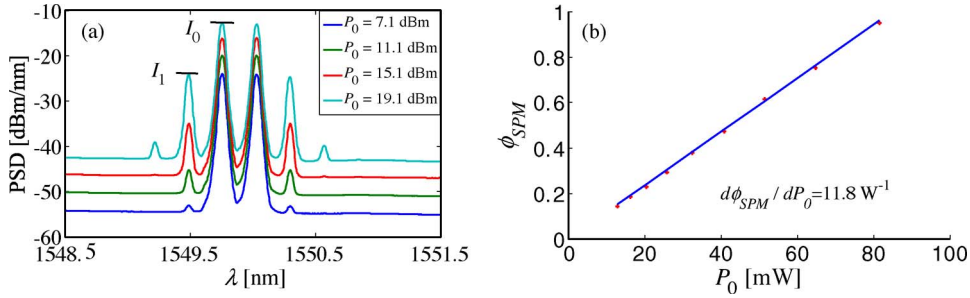

Fig. 9. Sinusoidal-signal self-phase modulation measurements showing (a) the recorded output spectra of the hybrid microtaper for increasing power levels and (b) the measured ϕ_{SPM} as a function of the peak power of the sinusoidal-signal.

Fig. 8 presents a schematic of the setup used to measure γ from the nonlinear phase-shift ϕ_{SPM} accumulated from signal propagation in the microwire [38]. A sinusoidal signal with a duration of 29 ps is formed by combining two continuous wave (CW) lasers at wavelengths $\lambda_1 = 1549.75$ nm and $\lambda_2 = 1550.03$ nm using a 3 dB coupler and then aligning their polarizations using two polarization controllers (PC), PC1 and PC2, and a linear polarizer (LP). The sinusoidal signal is amplitude modulated using a Mach–Zehnder modulator and a square pulse with a duration of 10 ns at a repetition rate of 1 MHz reducing the average power of the signal by 20 dB. The modulated signal is then amplified using an Erbium-doped fiber amplifier and passed to a variable attenuator (VA). The output of the attenuator is launched in the hybrid microtaper and the output of the microtaper is observed using an optical spectrum analyzer.

Fig. 9(a) shows the spectral evolution of the sinusoidal signal at the output of the hybrid microtaper at increasing peak power levels. Fig. 9(b) presents the value of ϕ_{SPM} for each peak power level calculated from I_0 and I_1, which are illustrated in Fig. 9, using the equation [38]

$$\frac{I_0}{I_1} = \frac{J_0^2(\phi_{SPM}/2) + J_1^2(\phi_{SPM}/2)}{J_1^2(\phi_{SPM}/2) + J_2^2(\phi_{SPM}/2)} \tag{1}$$

where J_0, J_1 and J_2 are the zero, first, and second order Bessel functions of the first kind. Using the experimentally estimated loss of 5.2 dB over the wire section length of 10 cm, the effective length is $L_{eff} = 5.83$ cm. The ratio of nonlinear phase-shift accumulating in the wire section $\phi_{SPM}^{w} = \gamma P_0 L_{eff}$ to the phase-shift in the entire microtaper $\phi_{SPM} = \int \gamma(z) P(z) dz$ is $\rho = \phi_{SPM}^{w}/\phi_{SPM} = 0.87$. The product $\gamma L_{eff}/\rho = 11.8$ W^{-1} is the slope of the linear fit connecting the experimentally measured values of ϕ_{SPM} in Fig. 9(b). The waveguide nonlinearity in the wire section of the microtaper is $\gamma = 11.8 \times \rho / L_{eff} = 176$ W^{-1}m^{-1}, in close agreement with the theoretically calculated value of 185 W^{-1}m^{-1} at $\phi_{AsSe} = 0.45$ μm in Fig. 4.

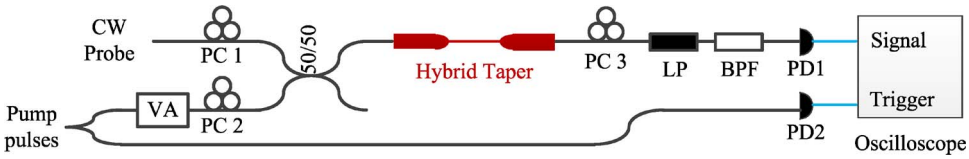

Fig. 10. Schematic of the Kerr-shutter setup. CW: continuous wave laser, PC: polarization controller, LP: linear polarizer, VA: variable attenuator, BPF: bandpass filter, PD: photodiode.

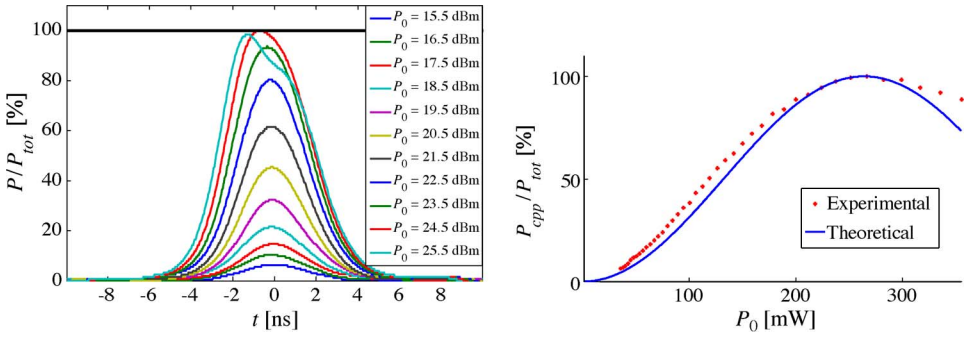

Fig. 11. Measured probe pulse at $\lambda = 1575$ nm showing (a) the probe pulse shape at increasing pump peak power levels, and (b) the power at the center of the converted pulse versus the peak power of the pump pulse.

6. All-Optical Switching in a Kerr-Shutter

Fig. 10 presents a schematic of the Kerr-shutter setup [27] used to demonstrate switching by induced polarization rotation in the hybrid microwire. Pump optical pulses with a full-width at half-maximum (FWHM) duration of $T_{FWHM} = 5.47$ ns and a repetition rate of $f = 3.3$ kHz at $\lambda = 1535$ nm from a Q-switched laser are combined with a CW laser probe at $\lambda = 1575$ nm using a 3 dB coupler and then launched into the microtaper. When the pump is linearly polarized in the microtaper and the pump peak-power is increased using the variable attenuator, birefringence is induced due to Kerr nonlinearity leading to time dependent birefringence modulation; consequently, the copropagating probe experiences polarization modulation. The polarization-modulated part of the probe is isolated using a linear polarizer which blocks the nonmodulated part of the probe leading to pulses at the probe wavelength. A tunable filter is then used to block the pump laser pulses and exclusively pass the probe pulses which are then detected using a photodiode and an oscilloscope. The polarization of the optical pulses from the Q-switched laser, the CW probe laser, and the output of the microtaper are adjusted using PC1, PC2, and PC3 such that the transmitted probe power is zero when the pump laser is OFF, and the peak of the probe pulse is maximum when the pump laser is ON.

The birefringence induced by the linearly polarized pump in the microtaper leads to a phase difference of $\Delta\phi_{Birefringence} = \phi_{SPM}$ between the parallel axis and the perpendicular axis to the pump. At the output of the linear polarizer aligned at 45° from the linearly polarized pump, the probe electric-field amplitude is given by $A_{out} = \sqrt{0.5}A_{\|}e^{-j\phi_{SPM}} - \sqrt{0.5}A_{\perp}$, where $A_{\|}$ and $A_{\perp}$ are the amplitudes of probe electric-field components parallel and perpendicular to the pump, respectively. Using $P_{\|} = |A_{\|}|^2 = rP_{tot}$ and $P_{\perp} = |A_{\perp}|^2 = (1-r)P_{tot}$, where $P_{\|}$ and $P_{\perp}$ are the powers of the probe components parallel and perpendicular to the pump, respectively, r is the ratio of the parallel probe component power to the total probe power, and $P_{tot} = P_{\|} + P_{\perp}$ is total probe power, the probe electric-field amplitude becomes $A_{out} = \sqrt{0.5P_{tot}}[\sqrt{r}e^{-j\phi_{SPM}/2} - \sqrt{(1-r)}e^{j\phi_{SPM}/2}]e^{-j\phi_{SPM}/2}$, and the probe power at the output of the linear polarizer becomes

$$P_{out} = 0.5P_{tot}\left[1 - 2\sqrt{r}\sqrt{(1-r)}\cos(\phi_{SPM})\right].$$

For $r = 0.5$ and using $\phi_{SPM} = \phi^{w}_{SPM}/\rho = \gamma P_0 L_{eff}/\rho$, the output probe power becomes $P_{out} = 0.5P_{tot}[1 - \cos(\gamma P_0 L_{eff}/\rho)]$ and full power switching occurs when the pump peak power P_0 reaches a critical power $P_c = \pi\rho/\gamma L_{eff}$.

Fig. 11(a) shows the probe pulse normalized to the total power of the probe P_{tot} that is measured at PD1 by adjusting PC3 until full probe transmission through the linear polarizer is achieved. Due to the quasi-CW nature of the long pump pulses, power at the center of the probe pulse (P_{cpp}) depends on the peak power P_0 at the center of the pump pulse following the relation $P_{cpp} = 0.5P_{tot}[1 - \cos(\gamma P_0 L_{eff}/\rho)]$. When P_0 reaches P_c, 100% power transmission occurs at the center of the probe pulse and P_{cpp} becomes equal to P_{tot}. As P_0 exceeds P_c, power transmission at the center of the probe pulse decreases while full power transmission occurs at the wings of the probe pulse. Consequently, a depression starts to appears at the center of probe pulse as can be observed in Fig. 11(a). Fig. 11(b) presents the measured power at center of the probe pulses as a function of the peak of the pump pulses. The power at the center of the probe pulse reaches maximum when the pump peak power is $P_0 = 266$ mW leading to $\gamma = \pi\rho/P_0 L_{eff} = 176\ \mathrm{W^{-1}m^{-1}}$ in agreement with the previous measurement. The estimated ratio $P_{cpp}/P_{tot} = 0.5[1 - \cos(\gamma P_0 L_{eff}/\rho)]$ is also plotted in Fig. 11(b) showing close agreement with experimental results.

7. Conclusion

A multimode As_2Se_3-PMMA fiber has been tapered to achieve single-mode transmission and an ultrahigh waveguide nonlinearity of $\gamma = 176\ \mathrm{W^{-1}m^{-1}}$. Fabrication of such hybrid microwires from a multimode As_2Se_3-PMMA fiber is greatly simplified as it eliminates the need for single-mode step-index As_2Se_3 fibers. Proper design of the initial As_2Se_3 diameter allowed for optimal power coupling into the microwire from an SMF. A Kerr-shutter has been implemented using the fabricated hybrid microwire to demonstrate switching by induced polarization rotation with a 100% switching power of 266 mW.

Acknowledgment

The authors are thankful to Coractive High-Tech for providing the As_2Se_3 cylinders used in this experiment.

References

[1] L. Yin, J. Zhang, P. M. Fauchet, and G. P. Agrawal, "Optical switching using nonlinear polarization rotation inside silicon waveguides," *Opt. Lett.*, vol. 34, no. 4, pp. 476–478, Feb. 2009.
[2] B. E. Olsson, P. Ohlen, L. Rau, and D. J. Blumenthal, "A simple and robust 40-Gb/s wavelength converter using fiber cross-phase modulation and optical filtering," *IEEE Photon. Technol. Lett.*, vol. 12, no. 7, pp. 846–848, Jul. 2000.
[3] J. K. Ranka, R. S. Windeler, and A. J. Stentz, "Visible continuum generation in air-silica microstructure optical fibers with anomalous dispersion at 800 nm," *Opt. Lett.*, vol. 25, no. 1, pp. 25–27, Jan. 2000.
[4] P. V. Mamyshev, "All-optical data regeneration based on self-phase modulation effect," in *Proc. 24th Eur. Conf. Opt. Commun.*, 1998, vol. 1, pp. 475–476.
[5] G. P. Agrawal, *Nonlinear Fiber Optics,* 4th ed. San Diego, CA: Academic, 2007.
[6] R. E. Slusher, G. Lenz, J. Hodelin, J. Sanghera, L. B. Shaw, and I. D. Aggarwal, "Large Raman gain and nonlinear phase shifts in high-purity As_2Se_3 chalcogenide fibers," *J. Opt. Soc. Amer. B, Opt. Phys.*, vol. 21, no. 6, pp. 1146–1155, Jun. 2004.
[7] T. Schreiber, J. Limpert, H. Zellmer, A. Tünnermann, and K. Hansen, "High average power supercontinuum generation in photonic crystal fibers," *Opt. Commun.*, vol. 228, no. 1–3, pp. 71–78, Dec. 2003.
[8] P. Dumais, F. Gonthier, S. Lacroix, J. Bures, A. Villeneuve, P. G. J. Wigley, and G. I. Stegeman, "Enhanced self-phase modulation in tapered fibers," *Opt. Lett.*, vol. 18, no. 23, pp. 1996–1998, Dec. 1993.
[9] K. Hansen, "Dispersion flattened hybrid-core nonlinear photonic crystal fiber," *Opt. Exp.*, vol. 11, no. 13, pp. 1503–1509, Jun. 2003.
[10] K. Kiang, K. Frampton, T. Monro, R. Moore, J. Tucknott, D. Hewak, D. Richardson, and H. Rutt, "Extruded singlemode non-silica glass holey optical fibres," *Electron. Lett.*, vol. 38, no. 12, pp. 546–547, Jun. 2002.
[11] E. C. Mägi, L. B. Fu, H. C. Nguyen, M. R. Lamont, D. I. Yeom, and B. J. Eggleton, "Enhanced Kerr nonlinearity in sub-wavelength diameter As_2Se_3 chalcogenide fiber tapers," *Opt. Exp.*, vol. 15, no. 16, pp. 10 324–10 329, Aug. 2007.
[12] C. Baker and M. Rochette, "Highly nonlinear hybrid AsSe-PMMA microtapers," *Opt. Exp.*, vol. 18, no. 12, pp. 12 391–12 398, Jun. 2010.
[13] L. Brilland, F. Smektala, G. Renversez, T. Chartier, J. Troles, T. Nguyen, N. Traynor, and A. Monteville, "Fabrication of complex structures of holey fibers in chalcogenide glass," *Opt. Exp.*, vol. 14, no. 3, pp. 1280–1285, Feb. 2006.

[14] M. El-Amraoui, J. Fatome, J. C. Jules, B. Kibler, G. Gadret, C. Fortier, F. Smektala, I. Skripatchev, C. Polacchini, Y. Messaddeq, J. Troles, L. Brilland, M. Szpulak, and G. Renversez, "Strong infrared spectral broadening in low-loss as-s chalcogenide suspended core microstructured optical fibers," *Opt. Exp.*, vol. 18, no. 5, pp. 4547–4556, Mar. 2010.
[15] S. D. Hart, G. R. Maskaly, B. Temelkuran, P. H. Prideaux, J. D. Joannopoulos, and Y. Fink, "External reflection from omnidirectional dielectric mirror fibers," *Science*, vol. 296, no. 5567, pp. 510–513, Apr. 2002.
[16] B. Temelkuran, S. D. Hart, G. Benoit, and J. D. J. Y. Fink, "Wavelength-scalable hollow optical fibres with large photonic bandgaps for CO_2 laser transmission," *Nature*, vol. 420, no. 6916, pp. 650–653, Dec. 2002.
[17] T. Engeness, M. Ibanescu, S. Johnson, O. Weisberg, M. Skorobogatiy, S. Jacobs, and Y. Fink, "Dispersion tailoring and compensation by modal interactions in omniguide fibers," *Opt. Exp.*, vol. 11, no. 10, pp. 1175–1196, May 2003.
[18] M. Liao, C. Chaudhari, G. Qin, X. Yan, C. Kito, T. Suzuki, Y. Ohishi, M. Matsumoto, and T. Misumi, "Fabrication and characterization of a chalcogenide-tellurite composite microstructure fiber with high nonlinearity," *Opt. Exp.*, vol. 17, no. 24, pp. 21 608–21 614, Nov. 2009.
[19] N. Granzow, S. P. Stark, M. A. Schmidt, A. S. Tverjanovich, L. Wondraczek, and P. S. Russell, "Supercontinuum generation in chalcogenide-silica step-index fibers," *Opt. Exp.*, vol. 19, no. 21, pp. 21 003–21 010, Oct. 2011.
[20] J. D. Love and W. M. Henry, "Quantifying loss minimisation in single-mode fibre tapers," *Electron. Lett.*, vol. 22, no. 17, pp. 912–914, Aug. 1986.
[21] J. D. Love, W. M. Henry, W. J. Stewart, R. J. Black, S. Lacroix, and F. Gonthier, "Tapered single-mode fibres and devices. I. adiabaticity criteria," *Proc. Inst. Elect. Eng.—J. Optoelectron.*, vol. 138, no. 5, pp. 343–354, Oct. 1991.
[22] F. Bilodeau, K. Hill, S. Faucher, and D. Johnson, "Low-loss highly overcoupled fused couplers: Fabrication and sensitivity to external pressure," in *Optical Fiber Sensors*. Washington, DC: Opt. Soc. Amer., 1988, p. ThC C10.
[23] F. Bilodeau, K. O. Hill, D. C. Johnson, and S. Faucher, "Compact, low-loss, fused biconical taper couplers: Overcoupled operation and antisymmetric supermode cutoff," *Opt. Lett.*, vol. 12, no. 8, pp. 634–636, Aug. 1987.
[24] S. Moon and D. Y. Kim, "Effective single-mode transmission at wavelengths shorter than the cutoff wavelength of an optical fiber," *Photon. Technol. Lett.*, vol. 17, no. 12, pp. 2604–2606, Dec. 2005.
[25] D. Donlagic, "In-line higher order mode filters based on long highly uniform fiber tapers," *J. Lightw. Technol.*, vol. 24, no. 9, pp. 3532–3539, Sep. 2006.
[26] Y. Jung, G. Brambilla, and D. J. Richardson, "Broadband single-mode operation of standard optical fibers by using a sub-wavelength optical wire filter," *Opt. Exp.*, vol. 16, no. 19, pp. 14 661–14 667, Sep. 2008.
[27] M. A. Duguay and J. W. Hansen, "An ultrafast light gate," in *IEDM Tech. Dig.*, 1969, vol. 15, pp. 68–70.
[28] C. Pollock and M. Lipson, *Integrated Photonics*. New York: Springer-Verlag, 2003.
[29] A. W. Snyder and J. D. Love, *Optical Waveguide Theory*. Boston, MA: Chapman & Hall, 1983.
[30] *AMTIR-2: Arsenic Selenide Glass As-Se,* 2009. [Online]. Available: http://www.amorphousmaterials.com/amtir2.htm
[31] S. N. Kasarova, N. G. Sultanova, C. D. Ivanov, and I. D. Nikolov, "Analysis of the dispersion of optical plastic materials," *Opt. Mater.*, vol. 29, no. 11, pp. 1481–1490, Jul. 2007.
[32] S. Afshar and T. M. Monro, "A full vectorial model for pulse propagation in emerging waveguides with subwavelength structures part I: Kerr nonlinearity," *Opt. Exp.*, vol. 17, no. 4, pp. 2298–2318, Feb. 2009.
[33] S. Afshar, W. Q. Zhang, H. Ebendorff-Heidepriem, and T. M. Monro, "Small core optical waveguides are more nonlinear than expected: Experimental confirmation," *Opt. Lett.*, vol. 34, no. 22, pp. 3577–3579, Nov. 2009.
[34] F. D'Amore, M. Lanata, S. M. Pietralunga, M. C. Gallazzi, and G. Zerbi, "Enhancement of PMMA nonlinear optical properties by means of a quinoid molecule," *Opt. Mater.*, vol. 24, no. 4, pp. 661–665, Jan. 2004.
[35] M. G. Kuzyk, *Polymer Fiber Optics: Materials, Physics, and Applications,* 1st ed. Boca Raton, FL: CRC, 2006.
[36] R. P. Kenny, T. A. Birks, and K. P. Oakley, "Control of optical fibre taper shape," *Electron. Lett.*, vol. 27, no. 18, pp. 1654–1656, Aug. 1991.
[37] T. A. Birks and Y. W. Li, "The shape of fiber tapers," *J. Lightw. Technol.*, vol. 10, no. 4, pp. 432–438, Apr. 1992.
[38] A. Boskovic, S. V. Chernikov, J. R. Taylor, L. Gruner-Nielsen, and O. A. Levring, "Direct continuous-wave measurement of n_2 in various types of telecommunication fiber at 1.55 μm," *Opt. Lett.*, vol. 21, no. 24, pp. 1966–1968, Dec. 1996.